nature climate change

ARTICLES

https://doi.org/10.1038/s41558-020-0763-7

Increasing contribution of peatlands to boreal evapotranspiration in a warming climate

Manuel Helbig[1,42]✉, James Michael Waddington[1], Pavel Alekseychik[2,3], Brian D. Amiro[4], Mika Aurela[5], Alan G. Barr[6,7], T. Andrew Black[8], Peter D. Blanken[9], Sean K. Carey[1], Jiquan Chen[10], Jinshu Chi[11], Ankur R. Desai[12], Allison Dunn[13], Eugenie S. Euskirchen[14], Lawrence B. Flanagan[15], Inke Forbrich[16], Thomas Friborg[17], Achim Grelle[18], Silvie Harder[19], Michal Heliasz[20], Elyn R. Humphreys[21], Hiroki Ikawa[22], Pierre-Erik Isabelle[23], Hiroki Iwata[24], Rachhpal Jassal[8], Mika Korkiakoski[5], Juliya Kurbatova[25], Lars Kutzbach[26], Anders Lindroth[27], Mikaell Ottosson Löfvenius[11], Annalea Lohila[2,5], Ivan Mammarella[2], Philip Marsh[28], Trofim Maximov[29], Joe R. Melton[30], Paul A. Moore[1], Daniel F. Nadeau[23], Erin M. Nicholls[1], Mats B. Nilsson[11], Takeshi Ohta[31], Matthias Peichl[11], Richard M. Petrone[32], Roman Petrov[29], Anatoly Prokushkin[33], William L. Quinton[28], David E. Reed[10], Nigel T. Roulet[19], Benjamin R. K. Runkle[26,34], Oliver Sonnentag[35], Ian B. Strachan[36], Pierre Taillardat[37], Eeva-Stiina Tuittila[38], Juha-Pekka Tuovinen[5], Jessica Turner[12], Masahito Ueyama[39], Andrej Varlagin[25], Martin Wilmking[40], Steven C. Wofsy[41] and Vyacheslav Zyrianov[33]

The response of evapotranspiration (ET) to warming is of critical importance to the water and carbon cycle of the boreal biome, a mosaic of land cover types dominated by forests and peatlands. The effect of warming-induced vapour pressure deficit (VPD) increases on boreal ET remains poorly understood because peatlands are not specifically represented as plant functional types in Earth system models. Here we show that peatland ET increases more than forest ET with increasing VPD using observations from 95 eddy covariance tower sites. At high VPD of more than 2 kPa, peatland ET exceeds forest ET by up to 30%. Future (2091–2100) mid-growing season peatland ET is estimated to exceed forest ET by over 20% in about one-third of the boreal biome for RCP4.5 and about two-thirds for RCP8.5. Peatland-specific ET responses to VPD should therefore be included in Earth system models to avoid biases in water and carbon cycle projections.

The boreal biome covers about one-eighth of the global terrestrial land surface area[1] and represents a mosaic of forest, peatland and lake ecosystems that comprise roughly 80%, 15% and 5% of the biome, respectively[2,3] (see Supplementary Fig. 1). Their total above- and below-ground organic carbon stocks of ~1,000 GtC (ref. [4]) together exceed the 860 GtC (ref. [5]) that is currently in the atmosphere. The largest soil organic carbon stocks are located in the regions with the highest peatland coverage (Supplementary Fig. 2) and these will adjust to a warming climate through enhanced soil organic matter decomposition[6], vegetation productivity[7], fire, and other natural and anthropogenic disturbances[8], all of which represent important global carbon–climate feedbacks[9]; however, the magnitude of these feedbacks is sensitive to changes in water availability[8,10] due to the strong coupling between the carbon and water cycle in plants, soils and the atmosphere[11]. Water availability for soil water recharge and discharge in the boreal biome is partly controlled by atmospheric water losses through evapotranspiration (ET), which comprises both evaporation and transpiration[12]. Accurate projections of future ET are therefore crucial for quantifying carbon–climate feedbacks in a warming climate[13].

Potential ET (PET) is driven by the available energy and the atmospheric vapour pressure deficit (VPD)[14], the latter of which is the difference between the saturation vapour pressure and the ambient vapour pressure and, as such, is a measure of atmospheric demand for water vapour. Globally, the VPD in the growing season (May to September) sharply increased after the late 1990s[15]. Increases in growing season mean daily maximum VPD (VPD_{GS}) of up to 10% have been observed in the boreal biome since the late 2000s (in comparison with the VPD_{GS} mean of 1981–2010, Extended Data Fig. 1). With a warming climate, the atmospheric demand for water vapour is expected to grow further due to a faster increase in the saturation vapour pressure—as per the Clausius–Clapeyron relationship—compared with vapour pressure[16]. Accordingly, Earth system models (ESMs) project an increase in VPD_{GS} at the end of the twenty-first century (2091–2100 relative to 2006–2015). A VPD_{GS} increase of $57 \pm 43\%$ (that is, 0.38 ± 0.29 kPa, median $\pm 1\sigma$) is projected for the boreal biome (Coupled Model Intercomparison Project 5 (CMIP5), see Supplementary Table 1 for data sources) under representative concentration pathway 8.5 (RCP8.5), in which anthropogenic greenhouse gas emissions continue to rise throughout the twenty-first century, whereas a VPD_{GS} increase of $25 \pm 11\%$ (that is, 0.17 ± 0.07 kPa) is projected for RCP4.5, in which emissions peak in 2040 and decline through the twenty-first century. The absolute magnitude of VPD_{GS} changes varies across the boreal

A full list of affiliations appears at the end of the paper.

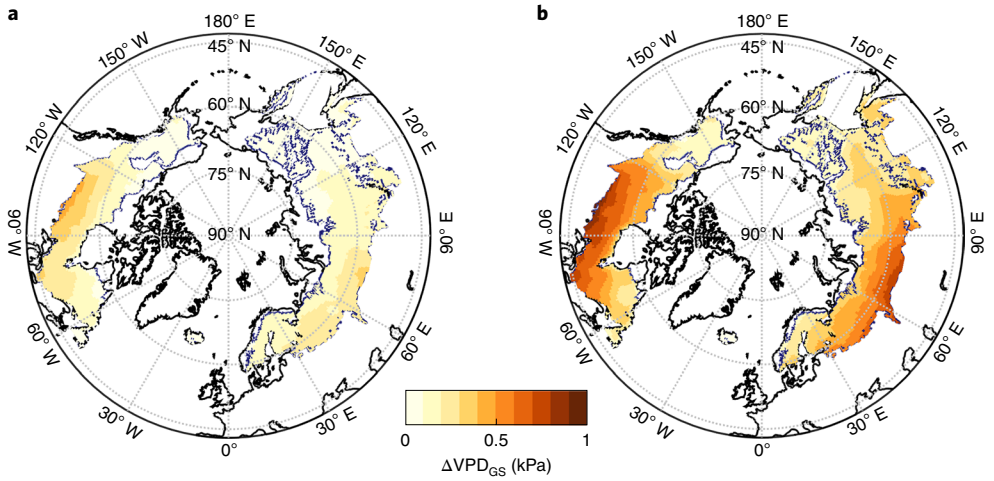

Fig. 1 | Multimodel mean projection of changes in growing season ΔVPD_{GS} by the end of the twenty-first century. a,**b**, Projections for the RCP4.5 (**a**) and RCP8.5 (**b**) scenarios are shown (years 2091–2100 versus 2006–2015, respectively). The output from eight CMIP5 ESMs (see Supplementary Table 1) was used to determine ΔVPD_{GS}.

biome and is generally most pronounced along its southern limit in western and central Canada and western and central Russia; it is least pronounced in Alaska, Scandinavia, eastern Canada and eastern Russia (see Fig. 1). Consequently, ecosystems across the boreal biome will be exposed to varying degrees of increasing atmospheric water vapour demand over the course of the twenty-first century.

Actual ET responses to VPD vary among ecosystems, mostly due to differences in aerodynamic (g_a) and surface conductance (g_s) for water vapour transfer[17–19]. For example, vascular plants (for instance, shrubs, trees) can limit water losses during periods of high VPD through physiological regulation mechanisms, whereas non-vascular plants (for example, bryophytes, such as mosses and lichens) lack such regulation[20,21]. To minimize water loss at times of high atmospheric demand for water, vascular plants reduce stomatal opening thereby reducing g_s (ref. [22]). The coverage of vascular and non-vascular plants varies greatly across the mosaic of boreal ecosystem types with high moss coverage in most peatlands[20,23]. Furthermore, in contrast to boreal forest ecosystems, the water table in peatlands is often close to the ground surface, providing ample water supply for ET. Values of g_s for water vapour transfer of peatland ecosystems may therefore be higher than those of boreal forest ecosystems[24]. Peatlands have recently been integrated into stand-alone offline versions of the land surface schemes from several ESMs[25–28], which has led to more accurate representation of peatland ET dynamics[28]; however, peatlands have yet to be included in future climate projections generated by those comprehensive coupled ESMs. As a result, ESMs continue to simulate the boreal region as an upland forest ecosystem[29] while not specifically accounting for peatlands. ET responses to a changing climate in the boreal biome therefore remain poorly constrained[30], hindering our ability to accurately project ET and hence soil moisture trends and carbon–climate feedbacks[31].

To evaluate how ET responds to a warmer climate with increasing atmospheric water demand across boreal ecosystems, we quantified relationships between ET and VPD using multiyear eddy covariance measurements from 60 forest and 35 peatland sites covering a wide range of the boreal climate space. These sites were generally characterized by a dryness index (that is, the ratio of annual PET to annual precipitation (P); data from ref. [32]) of <2.5 such that the VPD limitation of ET is expected to dominate soil moisture limitation[16] (Fig. 2). We found that, with an increase in VPD, ET increased more in boreal peatlands than in forests (Fig. 3), resulting in peatland ET exceeding forest ET by 30 ± 7% under a high VPD (>2 kPa). To quantify differences in ecosystem controls on ET, we derived afternoon g_s values under an optimal site-specific water supply and g_a values for these ecosystems from the eddy covariance measurements (see Methods); we found that ET differences between peatlands and forests were mainly driven by the higher g_s (mean $\Delta g_s = 1.9 \pm 0.5\,mm\,s^{-1}$) of peatlands. We estimated the differences between current and future mid-growing season ET for peatlands and forests under an optimal ecosystem-specific water supply and found that peatland ET exceeds forest ET across the boreal biome by an average of 5 ± 9% under current climatic conditions; however, under moderate (RCP4.5) and most severe (RCP8.5) warming scenarios, this percentage is expected to increase to 13 ± 11% and 28 ± 17%, respectively. This differential response will alter the boreal land surface energy balance with important implications for regional near-surface air temperatures and the development of boundary-layer clouds[33]. Furthermore, the projected water availability is likely to be overestimated by ESMs[34] in regions with large peatland coverage due to an underestimation of evaporative water losses. Greater ET increases in peatland-dominated regions may make them more prone to drying than boreal forest-dominated regions if precipitation changes are similar.

Instantaneous responses of peatland and forest ET to VPD

The ET and g_s responses to VPD were analysed using a boundary line analysis[35] (Methods). The upper envelope of the g_s relationship to VPD (Supplementary Fig. 3, Methods) only includes the highest g_s for a given VPD bin and thus removes limitations from other confounding environmental variables (for example, soil moisture, light). The differences in mean half-hourly peatland and forest ET increased with increasing VPD and reached a maximum of $0.13 \pm 0.03\,mm\,h^{-1}$ at VPD > 3 kPa (Fig. 3a,b). For VPD > 2 kPa, the mean peatland ET was about one-third larger than forest ET (30 ± 7%). Peatland and forest ET values were of similar magnitude only at a low VPD of <0.5 kPa. Similarly, peatland evaporative fraction (that is, the ratio of latent heat flux to the sum of latent and sensible heat flux) became increasingly larger than the forest evaporative fraction and reached maximum differences of about 60% for VPD > 2 kPa (0.68 for peatlands versus 0.42 for forests; Extended Data Fig. 2), indicating clear differences in energy partitioning between boreal peatlands and forests.

Higher peatland g_s compared with forest g_s was the main cause for larger peatland ET for the same atmospheric water demand. At high VPD (VPD > 2 kPa), the mean peatland g_s was 44 ± 9% higher

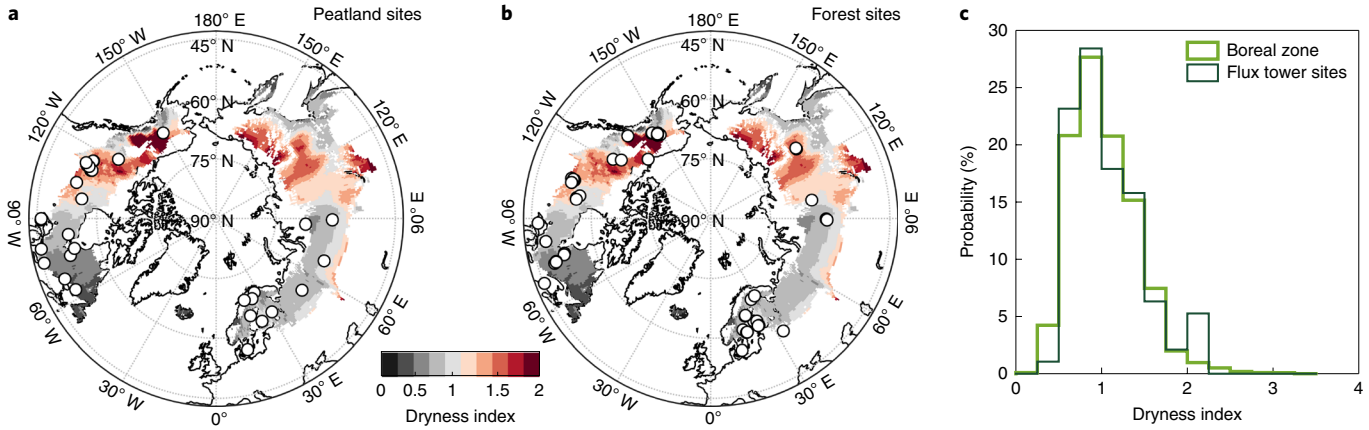

Fig. 2 | Eddy covariance flux tower locations and spatial pattern of dryness index in the boreal biome. a,**b**, The locations (circles) of peatland (**a**) and forest (**b**) eddy covariance flux towers in the boreal biome are shown. The colour scheme reflects the mean dryness index during 1981–2010. Data were obtained from the University of East Anglia Climate Research Unit Time-Series (CRU TS) v.4.02 (see Methods). **c**, The probability distribution of the dryness index is shown for the entire boreal biome (0.5 × 0.5° pixels from CRU TS v.4.02, $n = 10{,}515$) and for the flux tower sites ($n = 95$).

than forest g_s (Fig. 3c,d). The higher g_a of forests (Supplementary Fig. 4) had only a small effect on the ET–VPD response differences (Supplementary Fig. 5). We used the Penman–Monteith equation to model the peatland ET–VPD response to explore whether g_s or g_a is driving the observed difference in ET response (Methods). The root-mean-square error (r.m.s.e.) between modelled and observed peatland ET values was 0.06 mm h^{-1} when peatland ET was modelled using forest-specific g_s and peatland-specific g_a. The r.m.s.e. was reduced by 50% (0.03 mm h^{-1}) when peatland-specific g_s and forest-specific g_a was used, and further decreased to 0.01 mm h^{-1} when both peatland-specific g_s and g_a were used. These results highlight the importance of variations in g_s responses to atmospheric water demand within the boreal biome for accurate modelling of ET across the boreal biome in ESMs.

Increasing contribution of peatland ET in a warming climate

The mean observed cumulative growing season (May to September) peatland ET across all sites (280 ± 73 mm per growing season, $n = 122$ years, 26 sites, $P = 0.001$) was 11% higher than forest ET (252 ± 63 mm per growing season, $n = 305$ years, 55 sites, Extended Data Fig. 3), even with the mean growing season net radiation being slightly lower (105 W m^{-2} versus 114 W m^{-2}; $n_{PTL} = 115$ years, $n_{FOR} = 282$ years, $P = 0.003$). We accounted for the effects of the leaf area index (LAI) on forest g_s by scaling the g_s–VPD model using the satellite-derived mean July LAI (see Methods) to upscale the differential ET responses to VPD across the boreal biome. By contrast, peatland g_s–VPD model parameters did not depend on LAI, possibly due to the larger contribution of moss evaporation to total peatland ET[20]. Upscaled afternoon (15–18 h local time) peatland and forest ET in July (that is, mid-growing season) showed distinct spatial patterns, with peatland ET exceeding forest ET by about 10% in northwestern Canada and in northeastern Siberia under the current climate (Fig. 4). In a warming climate, peatland ET is expected to respond more strongly to increasing atmospheric water demand than forest ET. Peatland ET exceeds forest ET by more than 20% in only 21 ± 17% of the boreal biome under the current climate. In a warming climate, this area will expand to 33 ± 18% and 60 ± 24% for the RCP4.5 and RCP8.5 scenarios, respectively. For the RCP4.5 scenario, peatlands at the southern edge of the boreal biome in western and central Canada and in Russia are expected to experience enhanced evaporative water loss, whereas for the RCP8.5 scenario, peatland ET is expected to exceed forest ET by more than 20% in most of the boreal biome, with the exception of eastern and western coastal regions of North America and Eurasia.

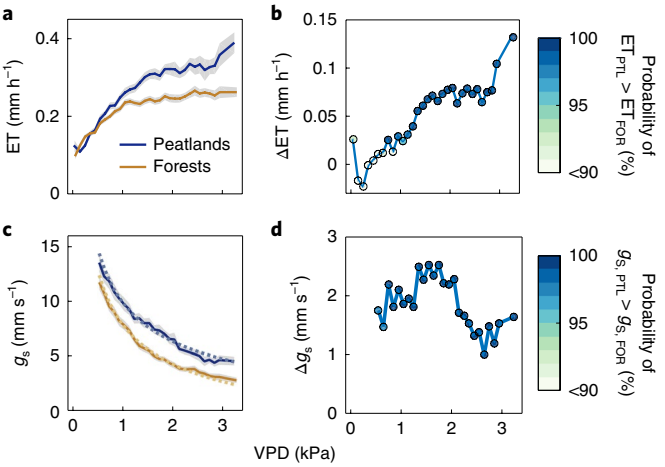

Fig. 3 | ET and g_s response to VPD. a, The mean half-hourly growing season ET responses of peatland and forest ecosystems to VPD (solid lines) are shown. The shaded areas indicate ±1 s.e.m. **b**, The mean difference between peatland (PTL) and forest (FOR) ET (ΔET) for each 0.1 kPa bin of measured VPD. The colours show the probability of peatland ET being higher than forest ET for the same VPD bin. **c**, The observed (solid lines) and fitted (dashed lines) g_s responses of peatland and forest ecosystems to VPD are shown. The shaded areas indicate ±1 s.e.m. **d**, The mean difference between peatland and forest g_s for each 0.1 kPa bin of measured VPD (for VPD > 0.5 kPa). The colours show the probability of peatland g_s being larger than forest g_s for the same VPD bin.

As such, not accounting for ecosystem-specific land surface properties of peatlands (as is common practice in coupled ESMs[29]) could lead to a considerable underestimation of evaporative water losses in peatland- and organic carbon-rich boreal regions such as the Hudson Bay Lowlands, Canada, and the Western Siberian Lowlands, Russia (Supplementary Fig. 2).

Accounting for peatlands in coupled ESMs

How future water availability will change in the boreal biome mainly depends on the balance between changes in P and ET; however, P and ET are tightly and coherently connected in the global climate system[36]. Larger peatland contributions to boreal ET in a warmer climate are likely to lead to complex interactions between the land surface and the atmosphere; for example, including a peatland land

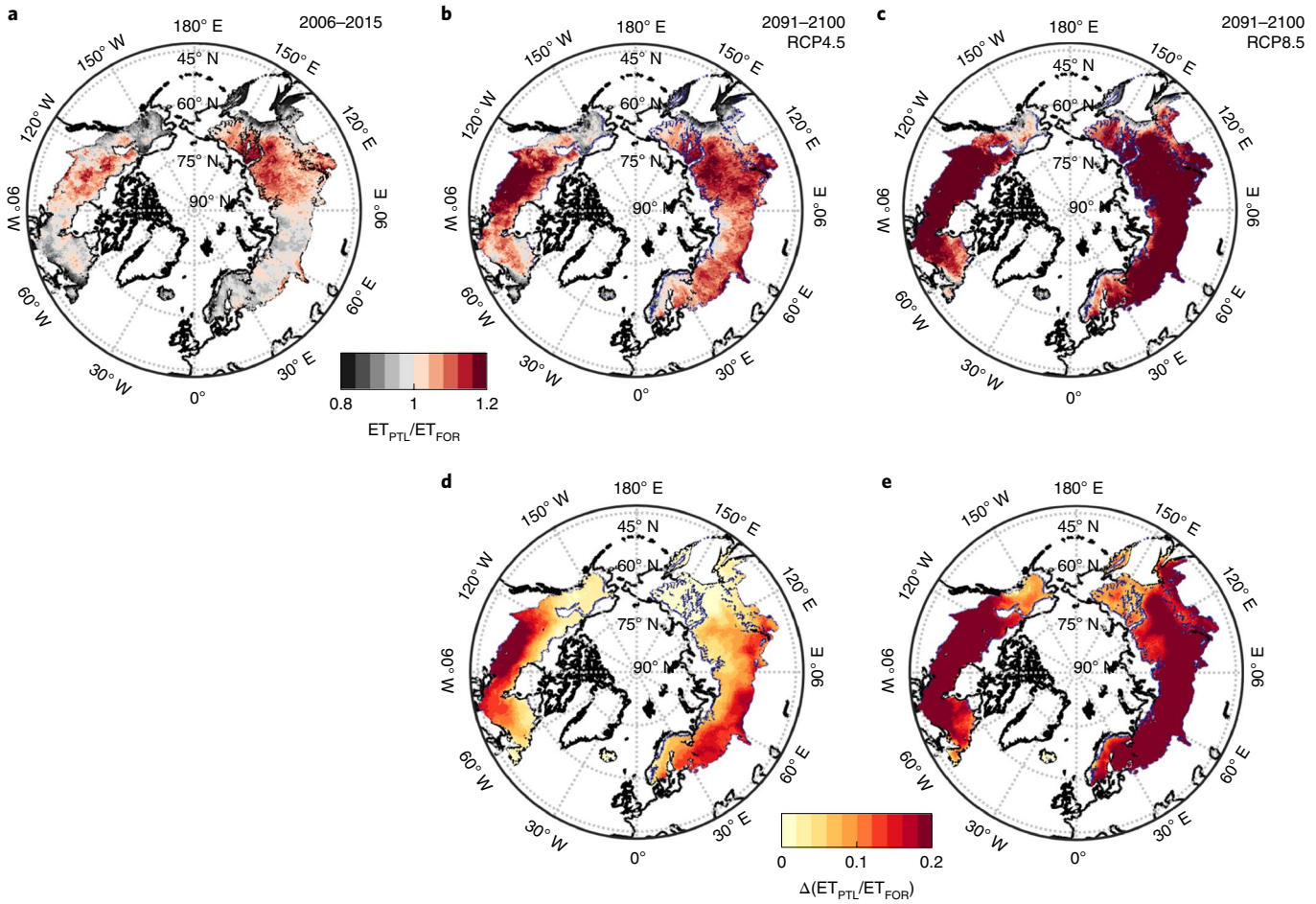

Fig. 4 | A comparison of peatland and forest ET under current and future climates. a–c, The ratio of afternoon (15–18 h) peatland (ET_{PTL}) to forest ET (ET_{FOR}) in July for the current climate (2006–2015) (**a**) and the RCP4.5 (**b**) and RCP8.5 (**c**) scenarios at the end of the twenty-first century (2091–2100). **d**,**e**, The increase in mid-growing season peatland-to-forest ET ratio at the end of the twenty-first century relative to the period 2006–2015 for the RCP4.5 (**d**) and RCP8.5 (**e**) scenarios.

cover type in a regional weather forecast model for the western Siberian Lowlands substantially altered ET estimates, near-surface air temperatures, boundary layer growth dynamics and consequently cloud type and cover[33]. An increase in evaporative fraction (Extended Data Fig. 2) may increase regional growing season P through greater atmospheric moisture and consequently higher probability of convective P[37,38]; however, a concurrent reduction in sensible heat fluxes would lead to shallower boundary layer depths limiting the occurrence of convective P events[39]. Furthermore, enhanced cloud cover would reduce the available energy at the ground surface[34] and potentially limit increases in ET due to reduced net radiation. Warming-induced changes in regional recycling of P are thus likely not fully captured by ESMs that prescribe a forest-only boreal biome that lacks subgrid peatland coverage. An underestimation of ET would also cause an underestimation of surface cooling[33,40,41], which could exert a negative feedback on VPD trends and lead to overestimation of atmospheric water demand in current climate projections. As such, there is a critical need to represent boreal peatland ecosystems in coupled ESMs to accurately simulate complex regional climate feedbacks arising from the exchange of water vapour between land and the atmosphere.

In addition to VPD limitations of ET[16], ET of vascular plant-dominated ecosystems is expected to be even further reduced by decreasing stomatal conductance with increasing atmospheric CO_2 concentrations[34]. For peatlands, much weaker ecophysiological responses to CO_2 and VPD are expected due to the lack of stomatal regulation of water vapour exchange in mosses[17,21] (Fig. 3c). Differences between changes in forest and peatland ET could therefore be even more pronounced than estimated in this study; however, the ability of boreal forests to conserve water more efficiently than peatlands during periods of high atmospheric demand may limit water stress in a warming climate more in the former than in the latter. Reduced water stress in forests could subsequently cause forest ET to exceed peatland ET during long-lasting heatwaves and droughts, similar to findings by Teuling et al.[42] for forests and grasslands. Peatland ET responses to VPD will also vary between peatland types that have site-specific water table dynamics and vascular plant and tree coverage[43]. Vascular plants are often more dominant in surface- or groundwater-fed fens than in rain-fed bogs[44,45]—the two most common peatland types in the boreal biome. Fens in this study are characterized by having a higher g_s than bogs (Supplementary Fig. 6); however, the decrease in g_s with increasing VPD is more pronounced in fens, suggesting a greater ecophysiological regulation of water losses. Thus, there will likely be limits to the magnitude of ET increase in fens relative to bogs due to the ability of fen-specific plant species to regulate their ecophysiological responses.

Water availability impacts in boreal peatlands and forests

Future projections for water availability in boreal ecosystems[34] are probably overestimated in current ESMs due to an underestimation

of ET. In a warming climate, increasing evaporative demand and potentially decreasing water availability will have adverse effects on vegetation productivity. Ecosystems may become less productive with increasing growing season VPD and lower water availability, particularly in regions already experiencing growing season water deficits[46]; however, forest and peatland responses will vary due to differences in plant species composition and their physiological characteristics (for example, rooting depth, LAI)[43,47,48]. More frequent drought occurrence could additionally lead to accelerated peatland carbon loss[49] and increased wildfire activity[8], particularly at the southern edge of the boreal biome.

If increasing peatland ET is not matched by an equivalent increase in precipitation, then storage and/or runoff will decrease. Drying could have adverse effects on peatland functioning[25]. Storage changes in bogs in particular would be reflected by a lowering of the absolute water table position due to the lack of groundwater or surface water inputs[50] and could potentially lead to the desiccation of the surface moss layer[51]. The magnitude of this water table decline is controlled by a number of ecohydrological feedbacks where decreasing surface moisture and lower canopy conductance can break the tight coupling between VPD and ET and reduce ET losses[52]. In some peatlands, the peat column compresses substantially with a lowering water table resulting in only small changes in water table position relative to surface height[53]. In these cases, the coupling between VPD and ET can remain strong, even during long-lasting drought periods[54]; however, greater canopy cover and a shift from the dominant moss vegetation to vascular vegetation can be expected as a result of a long-term lowering of the water table[55,56]. By contrast, recent permafrost thaw-induced increases in surface wetness and boreal forest loss have been observed in northwestern North America[57], resulting in increasing regional ET[24]. Furthermore, potential changes in soil water access due to warming soils and longer growing seasons[58] will additionally affect ET dynamics.

Our results reveal that peatland ET substantially exceeds forest ET across the boreal biome and that these differences are expected to increase under a warming climate. ESMs that do not account specifically for peatland-specific ecosystem properties thus underestimate evaporative water loss and overestimate current and future water availability, particularly in peatland-rich boreal regions. This bias can have important implications for projections of changing disturbance impacts (for example, changing fire regimes) and carbon cycling processes. Representing hydrological and ecophysiological characteristics specific to peatland ecosystems in ESMs will therefore probably improve their predictive capabilities for future climate change.

Online content

Any methods, additional references, Nature Research reporting summaries, source data, extended data, supplementary information, acknowledgements, peer review information; details of author contributions and competing interests; and statements of data and code availability are available at https://doi.org/10.1038/s41558-020-0763-7.

Received: 8 July 2019; Accepted: 26 March 2020;
Published online: 11 May 2020

References

1. Brandt, J. P., Flannigan, M. D., Maynard, D. G., Thompson, I. D. & Volney, W. J. A. An introduction to Canada's boreal zone: ecosystem processes, health, sustainability, and environmental issues. *Environ. Rev.* **21**, 207–226 (2013).
2. Verpoorter, C., Kutser, T., Seekell, D. A. & Tranvik, L. J. A global inventory of lakes based on high-resolution satellite imagery. *Geophys. Res. Lett.* **41**, 6396–6402 (2014).
3. Xu, J., Morris, P. J., Liu, J. & Holden, J. PEATMAP: refining estimates of global peatland distribution based on a meta-analysis. *CATENA* **160**, 134–140 (2018).
4. Bradshaw, C. J. A. & Warkentin, I. G. Global estimates of boreal forest carbon stocks and flux. *Glob. Planet. Change* **128**, 24–30 (2015).
5. Le Quéré, C. et al. Global carbon budget 2018. *Earth Syst. Sci. Data* **10**, 2141–2194 (2018).
6. Goulden, M. L. et al. Sensitivity of boreal forest carbon balance to soil thaw. *Science* **279**, 214–217 (1998).
7. Kauppi, P. E., Posch, M. & Pirinen, P. Large impacts of climatic warming on growth of boreal forests since 1960. *PLoS ONE* **9**, e111340 (2014).
8. Turetsky, M. R. et al. Global vulnerability of peatlands to fire and carbon loss. *Nat. Geosci.* **8**, 11–14 (2015).
9. Koven, C. D. Boreal carbon loss due to poleward shift in low-carbon ecosystems. *Nat. Geosci.* **6**, 452–456 (2013).
10. Allison, S. D. & Treseder, K. K. Warming and drying suppress microbial activity and carbon cycling in boreal forest soils. *Glob. Change Biol.* **14**, 2898–2909 (2008).
11. Gentine, P. et al. Coupling between the terrestrial carbon and water cycles—a review. *Environ. Res. Lett.* **14**, 083003 (2019).
12. Woo, M., Thorne, R., Szeto, K. & Yang, D. Streamflow hydrology in the boreal region under the influences of climate and human interference. *Philos. Trans. R. Soc. B* **363**, 2249–2258 (2008).
13. Fisher, J. B. et al. The future of evapotranspiration: global requirements for ecosystem functioning, carbon and climate feedbacks, agricultural management, and water resources. *Water Resour. Res.* **53**, 2618–2626 (2017).
14. Lafleur, P. M. & Rouse, W. R. The influence of surface cover and climate on energy partitioning and evaporation in a subarctic wetland. *Bound. Layer Meteorol.* **44**, 327–347 (1988).
15. Yuan, W. et al. Increased atmospheric vapor pressure deficit reduces global vegetation growth. *Sci. Adv.* **5**, eaax1396 (2019).
16. Novick, K. A. et al. The increasing importance of atmospheric demand for ecosystem water and carbon fluxes. *Nat. Clim. Change* **6**, 1023–1027 (2016).
17. Brümmer, C. et al. How climate and vegetation type influence evapotranspiration and water use efficiency in Canadian forest, peatland and grassland ecosystems. *Agric. For. Meteorol.* **153**, 14–30 (2012).
18. Barr, A. G., Betts, A. K., Black, T. A., McCaughey, J. H. & Smith, C. D. Intercomparison of BOREAS northern and southern study area surface fluxes in 1994. *J. Geophys. Res. Atmos.* **106**, 33543–33550 (2001).
19. Massmann, A., Gentine, P. & Lin, C. When does vapor pressure deficit drive or reduce evapotranspiration. *J. Adv. Model. Earth Syst.* **11**, 3305–3320 (2019).
20. Admiral, S. W. & Lafleur, P. M. Partitioning of latent heat flux at a northern peatland. *Aquat. Bot.* **86**, 107–116 (2007).
21. Williams, T. G. & Flanagan, L. B. Effect of changes in water content on photosynthesis, transpiration and discrimination against $^{13}CO_2$ and $C^{18}O^{16}O$ in *Pleurozium* and *Sphagnum*. *Oecologia* **108**, 38–46 (1996).
22. Oren, R. et al. Survey and synthesis of intra- and interspecific variation in stomatal sensitivity to vapour pressure deficit. *Plant Cell Environ.* **22**, 1515–1526 (1999).
23. Kellner, E. Surface energy fluxes and control of evapotranspiration from a Swedish *Sphagnum* mire. *Agric. For. Meteorol.* **110**, 101–123 (2001).
24. Helbig, M. et al. Regional atmospheric cooling and wetting effect of permafrost thaw-induced boreal forest loss. *Glob. Change Biol.* **22**, 4048–4066 (2016).
25. Chaudhary, N., Miller, P. A. & Smith, B. Modelling past, present and future peatland carbon accumulation across the Pan-Arctic region. *Biogeosciences* **14**, 4023–4044 (2017).
26. Qiu, C. et al. ORCHIDEE-PEAT (revision 4596), a model for northern peatland CO_2, water, and energy fluxes on daily to annual scales. *Geosci. Model Dev.* **11**, 497–519 (2018).
27. Wu, Y., Verseghy, D. L. & Melton, J. R. Integrating peatlands into the coupled canadian land surface scheme (class) v3.6 and the canadian terrestrial ecosystem model (CTEM) v2.0. *Geosci. Model Dev.* **9**, 2639–2663 (2016).
28. Bechtold, M. et al. PEAT-CLSM: a specific treatment of peatland hydrology in the NASA catchment land surface model. *J. Adv. Model. Earth Syst.* **11**, 2130–2162 (2019).
29. Poulter, B. et al. Plant functional type mapping for earth system models. *Geosci. Model Dev.* **4**, 993–1010 (2011).
30. Abramowitz, G., Leuning, R., Clark, M. & Pitman, A. Evaluating the performance of land surface models. *J. Clim.* **21**, 5468–5481 (2008).
31. Green, J. K. et al. Large influence of soil moisture on long-term terrestrial carbon uptake. *Nature* **565**, 476–479 (2019).
32. Harris, I., Jones, P. D., Osborn, T. J. & Lister, D. H. Updated high-resolution grids of monthly climatic observations—the CRU TS3.10 Dataset. *Int. J. Climatol.* **34**, 623–642 (2014).
33. Yurova, A., Tolstykh, M., Nilsson, M. & Sirin, A. Parameterization of mires in a numerical weather prediction model. *Water Resour. Res.* **50**, 8982–8996 (2014).
34. Lemordant, L., Gentine, P., Swann, A. S., Cook, B. I. & Scheff, J. Critical impact of vegetation physiology on the continental hydrologic cycle in response to increasing CO_2. *Proc. Natl Acad. Sci. USA* **115**, 4093–4098 (2018).

35. Ewers, B. E., Gower, S. T., Bond-Lamberty, B. & Wang, C. K. Effects of stand age and tree species on canopy transpiration and average stomatal conductance of boreal forests. *Plant Cell Environ.* **28**, 660–678 (2005).
36. Green, J. K. et al. Regionally strong feedbacks between the atmosphere and terrestrial biosphere. *Nat. Geosci.* **10**, 410–414 (2017).
37. Trenberth, K. E. Atmospheric moisture recycling: role of advection and local evaporation. *J. Clim.* **12**, 1368–1381 (1999).
38. Ford, T. W. & Frauenfeld, O. W. Surface–atmosphere moisture interactions in the frozen ground regions of Eurasia. *Sci. Rep.* **6**, 19163 (2016).
39. Konings, A. G., Katul, G. G. & Porporato, A. The rainfall–no rainfall transition in a coupled land-convective atmosphere system. *Geophys. Res. Lett.* **37**, L14401 (2010).
40. Sikma, M. & Vilà-Guerau de Arellano, J. Substantial reductions in cloud cover and moisture transport by dynamic plant responses. *Geophys. Res. Lett.* **46**, 1870–1878 (2019).
41. Bonan, G. B. Forests and climate change: forcings, feedbacks, and the climate benefits of forests. *Science* **320**, 1444–1449 (2008).
42. Teuling, A. J. et al. Contrasting response of European forest and grassland energy exchange to heatwaves. *Nat. Geosci.* **3**, 722–727 (2010).
43. Alekseychik, P. et al. Surface energy exchange in pristine and managed boreal peatlands. *Mires Peat* **20**, 1–26 (2018).
44. Zoltai, S. C. & Vitt, D. H. Canadian wetlands: environmental gradients and classification. *Vegetatio* **118**, 131–137 (1995).
45. Sulman, B. N. et al. CO_2 fluxes at northern fens and bogs have opposite responses to inter-annual fluctuations in water table. *Geophys. Res. Lett.* **37**, L19702 (2010).
46. Girardin, M. P. et al. Negative impacts of high temperatures on growth of black spruce forests intensify with the anticipated climate warming. *Glob. Change Biol.* **22**, 627–643 (2016).
47. Clenciala, E., Kucera, J., Ryan, M. G. & Lindroth, A. Water flux in boreal forest during two hydrologically contrasting years; species specific regulation of canopy conductance and transpiration. *Ann. Sci. For.* **55**, 47–61 (1998).
48. Helbig, M., Humphreys, E. R. & Todd, A. Contrasting temperature sensitivity of CO_2 exchange in peatlands of the Hudson Bay Lowlands, Canada. *J. Geophys. Res. Biogeosci.* **124**, 2126–2143 (2019).
49. Fenner, N. & Freeman, C. Drought-induced carbon loss in peatlands. *Nat. Geosci.* **4**, 895–900 (2011).
50. Charman, D. J. Summer water deficit variability controls on peatland water-table changes: implications for Holocene palaeoclimate reconstructions. *The Holocene* **17**, 217–227 (2007).
51. Rydin, H. Effect of water level on desiccation of *Sphagnum* in relation to surrounding *Sphagna*. *Oikos* **45**, 374–379 (1985).
52. Waddington, J. M. et al. Hydrological feedbacks in northern peatlands. *Ecohydrol.* **8**, 113–127 (2014).
53. Waddington, J. M., Kellner, E., Strack, M. & Price, J. S. Differential peat deformation, compressibility, and water storage between peatland microforms: Implications for ecosystem function and development. *Water Resour. Res.* **46**, W07538 (2010).
54. Nijp, J. J. et al. Including hydrological self-regulating processes in peatland models: Effects on peatmoss drought projections. *Sci. Total Environ.* **580**, 1389–1400 (2017).
55. Heijmans, M. M. P. D., van der Knaap, Y. A. M., Holmgren, M. & Limpens, J. Persistent versus transient tree encroachment of temperate peat bogs: effects of climate warming and drought events. *Glob. Change Biol.* **19**, 2240–2250 (2013).
56. Sulman, B. N., Desai, A. R. & Mladenoff, D. J. Modeling soil and biomass carbon responses to declining water table in a wetland-rich landscape. *Ecosystems* **16**, 491–507 (2013).
57. Carpino, O. A., Berg, A. A., Quinton, W. L. & Adams, J. R. Climate change and permafrost thaw-induced boreal forest loss in northwestern Canada. *Environ. Res. Lett.* **13**, 084018 (2018).
58. Buermann, W., Bikash, P. R., Jung, M., Burn, D. H. & Reichstein, M. Earlier springs decrease peak summer productivity in North American boreal forests. *Environ. Res. Lett.* **8**, 024027 (2013).

[1]School of Geography and Earth Sciences, McMaster University, Hamilton, Ontario, Canada. [2]Department of Physics, University of Helsinki, Helsinki, Finland. [3]Natural Resources Institute Finland (LUKE), Helsinki, Finland. [4]Department of Soil Science, University of Manitoba, Winnipeg, Manitoba, Canada. [5]Finnish Meteorological Institute, Helsinki, Finland. [6]Climate Research Division, Environment and Climate Change Canada, Saskatoon, Saskatchewan, Canada. [7]Global Institute for Water Security, University of Saskatchewan, Saskatoon, Saskatchewan, Canada. [8]Faculty of Land and Food Systems, The University of British Columbia, Vancouver, British Columbia, Canada. [9]Department of Geography, University of Colorado, Boulder, CO, USA. [10]Department of Geography, Environment, and Spatial Sciences, Michigan State University, East Lansing, MI, USA. [11]Department of Forest Ecology and Management, Swedish University of Agricultural Sciences, Umea, Sweden. [12]Department of Atmospheric and Oceanic Sciences, University of Wisconsin–Madison, Madison, WI, USA. [13]Department of Earth, Environment, and Physics, Worcester State University, Worcester, MA, USA. [14]Institute of Arctic Biology, University of Alaska Fairbanks, Fairbanks, AK, USA. [15]Department of Biological Sciences, University of Lethbridge, Lethbridge, Alberta, Canada. [16]The Ecosystems Center, Marine Biological Laboratory, Woods Hole, MA, USA. [17]Department of Geosciences and Natural Resource Management, University of Copenhagen, Copenhagen, Denmark. [18]Department of Ecology, Swedish University of Agricultural Sciences, Uppsala, Sweden. [19]Department of Geography, McGill University, Montréal, Québec, Canada. [20]Centre for Environmental and Climate Research, Lund University, Lund, Sweden. [21]Department of Geography and Environmental Studies, Carleton University, Ottawa, Ontario, Canada. [22]Institute for Agro-Environmental Sciences National Agriculture and Food Research Organization, Tsukuba, Japan. [23]Département de Génie Civil et de Génie des Eaux, Université Laval, Québec City, Québec, Canada. [24]Department of Environmental Science, Shinshu University, Matsumoto, Japan. [25]A.N. Severtsov Institute of Ecology and Evolution, Russian Academy of Sciences, Moscow, Russia. [26]Institute of Soil Science, University of Hamburg, Hamburg, Germany. [27]Department of Physical Geography and Ecosystem Science, Lund University, Lund, Sweden. [28]Cold Regions Research Centre, Wilfrid Laurier University, Waterloo, Ontario, Canada. [29]Institute for Biological Problems of Cryolithozone, Siberian Branch of the Russian Academy of Sciences, Yakutsk, Russia. [30]Climate Research Division, Environment and Climate Change Canada, Victoria, British Columbia, Canada. [31]Graduate School of Bioagricultural Sciences, Nagoya University, Nagoya, Japan. [32]Department of Geography and Environmental Management, University of Waterloo, Waterloo, Ontario, Canada. [33]V.N. Sukachev Institute of Forest, Siberian Branch of the Russian Academy of Sciences, Krasnoyarsk, Russia. [34]Department of Biological and Agricultural Engineering, University of Arkansas, Fayetteville, AR, USA. [35]Département de Géographie and Centre d'Études Nordiques, Université de Montréal, Montréal, Québec, Canada. [36]Department of Natural Resource Sciences, McGill University, Sainte-Anne-de-Bellevue, Québec, Canada. [37]Université du Québec à Montréal—Geotop, Montréal, Québec, Canada. [38]School of Forest Sciences, University of Eastern Finland, Joensuu, Finland. [39]Graduate School of Life and Environmental Sciences, Osaka Prefecture University, Sakai, Japan. [40]Institute of Botany and Landscape Ecology, University of Greifswald, Greifswald, Germany. [41]Department of Earth and Planetary Sciences, Harvard University, Cambridge, MA, USA. [42]Present address: Department of Physics and Atmospheric Science, Dalhousie University, Halifax, Nova Scotia, Canada. ✉e-mail: mhelbig85@gmail.com

Methods

Study sites and data processing. We use half-hourly eddy covariance measurements of ET at 35 peatland and 60 forest (deciduous and evergreen needleleaf forest, mixed forest, deciduous broadleaf forest, shrubland) flux tower sites across the boreal biome (Supplementary Data). The peatland subdataset includes 15 ombrotrophic bogs and 19 minerogenic fens. One peatland flux tower (FI-SAL) had changing source areas over a fen and a bog depending on wind direction. Most sites are climatologically hygric and mesic sites. At about half of the sites (51%), annual P exceeds annual PET, resulting in a dryness index (dryness index = PET/P) of less than one. This fraction compares well with the entire boreal biome, in which 53% of the area is characterized by dryness index of <1. The distribution of dryness index across the flux tower locations and across the entire boreal biome (0.5° × 0.5°, data from University of East Anglia CRU TS v.4.02; ref. [32]) was not significantly different ($P = 0.68$; two-sample Kolmogorov–Smirnov test, see Fig. 2). The dryness index of flux tower sites ranged from 0.4 to 2.2 (median dryness index = 0.96) and the median long-term (1981–2010) dryness index of peatland sites (0.86, $n = 35$) was not significantly different ($P = 0.19$, Wilcoxon rank sum test) from the dryness index of forests (1.04, $n = 60$, Supplementary Fig. 7). Similarly, the median annual long-term (1981–2010) PET of peatland sites (486 mm, $n = 35$) was not significantly different ($P = 0.86$, Wilcoxon rank sum test) from the PET of forests (507 mm, $n = 60$, Supplementary Fig. 7). The latitudinal distribution of peatland and forest flux tower sites was not significantly different (two-sample Kolmogorov–Smirnov test, $P = 0.55$). The median growing season incoming shortwave radiation ($P = 0.17$, $n_{PTL} = 122$, $n_{FOR} = 302$) and growing season air temperature ($P = 0.97$, $n_{PTL} = 164$, $n_{FOR} = 381$) measured at the eddy covariance tower sites were not significantly different between peatland and forest sites. Peatland and forest sites were classified based on vegetation class as reported in the flux tower site metadata. Some sites are located just south of the boreal biome as delineated by ref. [59] (Fig. 2). We have included these sites in our study to better cover the southern ecotone of the boreal biome[60].

In total, 2,431 growing season ET site months (May to September; peatlands, 723; forests, 1,708) were analysed. We used quality assurance/quality control and friction velocity threshold information from FLUXNET2015 and AmeriFlux datasets to ensure high-quality flux data (that is, stationary conditions, well developed turbulence, no sensor malfunction)[61]. For datasets not drawn from these databases ($n = 57$), we applied a friction velocity threshold algorithm and a median absolute deviation filter to detect outliers according to ref. [61]. If site-specific friction velocity thresholds were reported in the literature, these thresholds were used to filter ET. The median of reported energy balance closures for peatland sites was 0.87 ± 0.11 ($n = 18$) and not significantly different (Wilcoxon rank sum test, $P = 0.22$) from forests (0.87 ± 0.10, $n = 39$). Gaps in the ET time-series were filled using a marginal distribution sampling algorithm[62] using incoming shortwave radiation, air temperature and VPD as look-up variables. Gap-filled time-series were used to estimate growing season totals of ET. All other analyses were conducted using non-gap-filled time-series. Meteorological variables were not gap-filled. For the entire boreal biome, monthly P, monthly maximum VPD (derived from the mean daily vapour pressure and the mean daily maximum air temperature) and PET were derived from the CRU TS dataset (v.4.02) with a 0.5° resolution for 1981–2017. PET was calculated using a variant of the Penman–Monteith method with a g_s of 14 mm s^{-1} and an assumed surface albedo of 0.23 (ref. [32]).

Derivation of g_s and g_a. Vegetation influences ET through its effect on g_s and g_a. Both conductances can be derived from eddy covariance flux data; g_a was derived as follows including an approximation of the excess resistance to water vapour transport[63,64],

$$g_a = \left(\frac{kB^{-1}}{ku_*} \left(\frac{d_h}{d_v} \right)^{\frac{2}{3}} + \frac{U}{u_*^2} \right)^{-1}$$

where $k = 0.4$ is von Karman's constant, B^{-1} is a non-dimensional bulk parameter, u_* is the friction velocity, U is the mean wind speed, d_h is the thermal diffusivity and d_v is the molecular diffusivity of water vapour; d_h/d_v is 0.89 at 20 °C. Under near-neutral conditions, kB^{-1} can be approximated as the logarithm of the ratio of the momentum roughness length to the sensible heat roughness length and is assumed to be 2 for this study (as it is in ref. [63]); g_s includes stomatal conductance and conductance of wet surfaces (for example, moss and vascular plant surfaces) and was derived by inverting the Penman–Monteith equation[16,63]:

$$\frac{1}{g_s} = \left(\frac{s}{\gamma} \left(\frac{R_a}{\lambda ET} - 1 \right) - 1 \right) g_a^{-1} + \frac{\rho c_p VPD}{\gamma \lambda ET}$$

where R_a is the available energy (that is, the sum of sensible and latent heat flux); s is the change in saturation vapour pressure with temperature; λ is the latent heat of evaporation; γ is the psychrometric constant; and ρ and c_p are the density and specific heat capacity of air, respectively. We derived g_s only for the period between 15 h and 18 h local time that coincided with the mean timing of the peak VPD across all sites (Supplementary Fig. 8). Furthermore, g_s was only derived for periods with sufficiently high energy fluxes ($\lambda ET > 50$ W m^{-2} and available energy $R_a > 100$ W m^{-2}) to ensure numerical robustness.

Instantaneous ET– and g_s–VPD sensitivity analysis. At annual and seasonal scales, VPD and soil moisture are often correlated[16]. A strong VPD-soil moisture correlation could mask any direct ET response to VPD. At subdaily timescales, VPD and soil moisture are only weakly correlated[16]. We therefore analysed the half-hourly ET and g_s to better understand dynamic peatland and forest ET responses to VPD.

We applied a boundary line analysis (see Supplementary Fig. 3 for example) to study the instantaneous growing season response of ET and g_s to VPD at each site, which removes confounding effects of other environmental variables (that is, assuming g_s values lower than the boundary line values are limited by light availability, soil moisture, LAI and so on[35]). We assume that the g_s responses to VPD presented in this study do not account for limitations due to soil moisture anomalies and only relate to site-specific g_s responses to increasing atmospheric water demand.

Half-hourly growing season ET and g_s were binned for peatland and forest sites separately into 31 VPD-bins with a width of 0.1 kPa. VPD calculations were based on measurements of air temperature and humidity co-located with eddy covariance flux measurements. As we are mainly interested in the g_s response to VPD, the upper boundary was defined using g_s data. First, g_s outliers were identified and removed from each bin by applying the interquartile rule: outliers are flagged as all of the data points that are smaller than 25th percentile – 1.5 × interquartile range (that is, the 75th to 25th percentile) and larger than 75th percentile + 1.5 × interquartile range. Second, for each VPD bin, the upper boundary of g_s was defined as all half hours when $g_s >$ mean $g_s + 1\sigma$ following ref. [35]. The upper boundary of ET was defined as ET measurements that coincide with the upper boundary of g_s. We therefore assume that the ET response presented in this study is not driven by wind speed effects on g_a. We derived the probability of peatland ET (and g_s) exceeding forest ET (and g_s) by applying a permutation test with 1,000 permutations for each VPD bin. We also tested whether available energy differences may cause the different ET responses to VPD and found that there were no differences between available energy in peatlands and forests at VPD > 1 kPa (Supplementary Fig. 9).

The g_s–VPD relationship was approximated by fitting the following empirical model to the upper boundary of g_s:

$$g_s = g_0 + \left(1 + \frac{g_1}{\sqrt{VPD}} \right)$$

This parameterization of the g_s–VPD relationship is similar to the approximation of optimal stomatal conductance[65] but does not include a carbon uptake (that is, photosynthesis) term. In peatlands, non-vascular mosses without stomatal regulation often substantially contribute to ecosystem-scale carbon uptake[66]. The photosynthesis term was therefore not included in the empirical g_s model. Additionally, variability in g_s due to varying carbon uptake rates is expected to be minimized by applying a boundary line analysis. Model parameters g_0 and g_1 were derived using only data when VPD was > 1.0 kPa to avoid unstable g_s estimates when derived by dividing by near-zero VPD[16]. Median peatland g_0 (-2.3 ± 3.0 mm s^{-1}) was 2.8 mm s^{-1} higher than for forests (-5.1 ± 2.4 mm s^{-1}), whereas the median slope parameter g_1 was not different (11.4 ± 5.5 mm s^{-1} kPa versus 11.8 ± 3.8 mm s^{-1} kPa, Supplementary Fig. 10). Median coefficients of determination of the model fits for peatlands and forests were 0.80 and 0.87, respectively, and the r.m.s.e. were 0.12 mm s^{-1} and 0.07 mm s^{-1}, respectively.

Ecosystem-scale g_s is expected to be partly dependent on LAI for vascular plant-dominated ecosystems; however, a decrease in plant transpiration at the expense of soil evaporation with decreasing LAI may lead to lower sensitivity of g_s to LAI[67]. For all flux tower sites, the satellite-based LAI was derived from the moderate resolution imaging spectroradiometer (MODIS) eight-day LAI product (MCD15A2H[68]) with a spatial resolution of 500 m. A monthly averaged eight-day LAI for July was used for the entire MODIS observation period (July 2002 to 2018) to test whether g_s–VPD model parameters scale with observed LAI. Both g_0 and g_1 for forests scaled with mid-growing season LAI but peatland parameters were not correlated to LAI (Supplementary Fig. 11). Denser boreal forests were characterized by higher g_s at low VPD and higher sensitivity to increasing VPD in comparison with low LAI forests (Supplementary Fig. 12). This LAI effect on forest g_s was included when upscaling ET by scaling the forest fit parameters g_0 and g_1 using a satellite-derived LAI climatology[69].

Calculating current and future peatland-to-forest ET ratios. Boreal peatland and forest ET during the mid-growing season were estimated for the entire boreal biome using current (2006–2015) and projected future (2091–2100) mean daily maximum VPD (RCP4.5 and RCP8.5) for July. At 76% of the flux tower sites, July was the month with the highest monthly ET. Peak VPD during the day is usually reached between 15 h and 18 h (Supplementary Fig. 8) and our ET estimates therefore represent afternoon ET rates. Afternoon ET is usually a good predictor of daily ET and explained on average 91% ± 3% of the variability in daily ET rates in July across all flux tower sites. The Penman–Monteith equation was used to calculate ET:

$$\lambda ET = \frac{s R_a + \rho c_p VPD g_a}{s + \gamma \left(1 + \frac{g_a}{g_s} \right)}$$

Current VPD was derived from the CRU TS dataset (2006–2015), whereas the projected ΔVPD (that is, the difference between maximum July VPD for the periods 2091–2100 and 2006–2015) was added to current VPD to derive future VPD. VPD time-series were calculated using ESM simulations of daily specific humidity, maximum air temperature and atmospheric pressure to derive ΔVPD, as described in ref. [70].

Afternoon available energy (R_a, 15–18 h in July) was estimated as follows:

1. We used the global FLUXCOM land–atmosphere energy flux product[71] to estimate R_a (that is, the sum of sensible and latent heat flux) under current climatic conditions for each 0.5° grid cell. We used daily mean R_a for July for the ten-year period from 2004 to 2013; 2013 is the most recent year with FLUXCOM coverage.
2. We applied empirical relationships between mean daily and mean afternoon R_a derived from eddy covariance flux tower measurements (across all sites: $r^2 = 0.63 \pm 0.15$, $n = 75$) to estimate afternoon R_a. First we tested whether there was a difference in the mean daily R_a between peatland and forest sites. The mean daily peatland R_a (109 W m^{-2}, $n_{PTL} = 33$) was not significantly different from mean daily forest R_a (106 W m^{-2}, $n_{FOR} = 57$; Wilcoxon rank sum test: $P = 0.78$). Mean afternoon R_a was 12% lower for peatlands (235 W m^{-2}) than for forests (266 W m^{-2}), but the difference was not statistically significant (Wilcoxon rank sum test: $P = 0.06$). Differences in afternoon R_a may be due to larger ground heat fluxes in peatlands. We applied separate empirical relationships between mean daily and mean afternoon R_a for peatlands and forests to account for this potential difference in available energy.
3. We derived projected relative changes in R_a (%) from CMIP5 model runs of eight ESMs (RCP4.5 and RCP8.5 scenario, see Supplementary Table 1). The relative R_a changes were then applied to recent R_a to estimate future R_a (2091–2100). Empirical relationships between mean daily and mean afternoon R_a were applied to estimate mean afternoon R_a for peatlands and forests.

g_s was modelled as a function of VPD (equation 3). Model parameters g_0 and g_1 were scaled for boreal forests (Supplementary Fig. 11) using mean July LAI from a global mean monthly LAI climatology product[69] (1981–2015, 0.25° × 0.25° resolution). The mean afternoon (15–18 h) g_a was derived for each site as described above.

Uncertainties in current and projected ET estimates due to uncertainties in VPD and in R_a projections and in g_a and g_s parameterization were calculated as follows:

1. We used ΔVPD and ΔR_a using model outputs from eight ESMs (Supplementary Table 1).
2. We randomly selected g_a from the set of g_a estimates across all peatland and forest sites (120 times per ESM output).
3. For peatlands, we randomly selected from a normal distribution of peatland parameters for the g_s–VPD function (median $\pm 1\sigma$, 120 times per ESM output), whereas, for forests, we first scaled forest g_s–VPD parameters using the observed LAI relationship and then added a random sample from the normal distribution of the r.m.s.e. of the LAI relationship (120 times per ESM output).
4. The interquartile range of the differences in peatland and forest ET estimates was then derived for each pixel on the basis of the 960 simulations (that is, 8 ESMs × 120 parameter samples, Supplementary Fig. 13); these simulations were also used to calculate the areal fraction of the boreal biome (and its uncertainty) in which modelled peatland ET exceeds forest ET by more than 20% for the current climate, RCP4.5 and RCP8.5, as well as its s.d.

Data availability

Source data for Figs. 1–4 and Extended Data Figs. 1–3 are provided with the paper. Eddy covariance flux tower data used in this study can be accessed through the AmeriFlux (https://ameriflux.lbl.gov/), FLUXNET (https://fluxnet.fluxdata.org/data/fluxnet2015-dataset/), or European Fluxes Database Cluster (http://www.europe-fluxdata.eu/) webpages (see Supplementary Data). Site data that are not accessible through these webpages (see Supplementary Data) are available from the corresponding author on request. Monthly climate data and PET can be accessed through the East Anglia Climate Research Unit webpage (https://crudata.uea.ac.uk/cru/data/hrg/cru_ts_4.02/). Most CMIP5 model output is archived and made available through the Earth System Grid Federation (https://esgf.llnl.gov/). CanESM2 model output can be downloaded through the Canadian Centre for Climate Modelling and Analysis (http://climate-modelling.canada.ca/data/cgcm4/CanESM2/index.shtml) and CESM1-CAM5 model output is available through the Climate Data Gateway at the National Center for Atmospheric Research (https://www.earthsystemgrid.org/). Peatland maps are freely available through the Research Data Leeds Repository (http://archive.researchdata.leeds.ac.uk/251/) and on request from the corresponding author. MODIS data can be accessed for all flux tower sites through the Global Subset Tool: MODIS/VIIRS Products (https://modis.ornl.gov/cgi-bin/MODIS/global/subset.pl). The global FLUXCOM land-atmosphere energy flux data product can be accessed through the FLUXCOM webpage (http://www.fluxcom.org/EF-Products/). Global monthly mean LAI climatology can be accessed through the ORNL Distributed Active Archive Center for Biogeochemical Dynamics (https://daac.ornl.gov/VEGETATION/guides/Mean_Seasonal_LAI.html).

Code availability

All MATLAB code used in this study is available through the corresponding author's GitHub repository[72] (https://github.com/manuelhelbig/BWF_Synthesis; https://doi.org/10.5281/zenodo.3653056) and is available from the corresponding author on request. The software used to generate all results is MATLAB 2016a.

References

59. Olson, D. M. et al. Terrestrial ecoregions of the world: a new map of life on Earth. *BioScience* **51**, 933–938 (2001).
60. Hollinger, D. Y. et al. Seasonal patterns and environmental control of carbon dioxide and water vapour exchange in an ecotonal boreal forest. *Glob. Change Biol.* **5**, 891–902 (1999).
61. Papale, D. et al. Towards a standardized processing of net ecosystem exchange measured with eddy covariance technique: algorithms and uncertainty estimation. *Biogeosciences* **3**, 571–583 (2006).
62. Reichstein, M. et al. On the separation of net ecosystem exchange into assimilation and ecosystem respiration: review and improved algorithm. *Glob. Change Biol.* **11**, 1424–1439 (2005).
63. Humphreys, E. R. et al. Summer carbon dioxide and water vapor fluxes across a range of northern peatlands. *J. Geophys. Res. Biogeosciences* **111**, G04011 (2006).
64. Verma, S. B. *Aerodynamic Resistances to Transfers of Heat, Mass and Momentum* (eds Black, T. A. et al.) Vol. 177, 13–20 (International Association of Hydrological Sciences, 1989); http://hydrologie.org/redbooks/a177/iahs_177_0013.pdf
65. Medlyn, B. E. et al. Reconciling the optimal and empirical approaches to modelling stomatal conductance. *Glob. Change Biol.* **17**, 2134–2144 (2011).
66. Moore, T. R., Bubier, J. L., Frolking, S. E., Lafleur, P. M. & Roulet, N. T. Plant biomass and production and CO_2 exchange in an ombrotrophic bog. *J. Ecol.* **90**, 25–36 (2002).
67. Kelliher, F. M., Leuning, R., Raupach, M. R. & Schulze, E.-D. Maximum conductances for evaporation from global vegetation types. *Agric. For. Meteorol.* **73**, 1–16 (1995).
68. Myneni, R., Knyazikhin, Y. & Park, T. *MOD15A2H v006: MODIS/Terra Leaf Area Index/FPAR 8-Day L4 Global 500 m SIN Grid* (NASA, 2015); https://doi.org/doi:10.5067/MODIS/MOD15A2H.006
69. Mao, J. & Yan, B. *Global Monthly Mean Leaf Area Index Climatology, 1981–2015* (ORNL DAAC, 2019); https://doi.org/10.3334/ORNLDAAC/1653
70. Ficklin, D. L. & Novick, K. A. Historic and projected changes in vapor pressure deficit suggest a continental-scale drying of the United States atmosphere. *J. Geophys. Res. Atmospheres* **122**, 2061–2079 (2017).
71. Jung, M. et al. The FLUXCOM ensemble of global land-atmosphere energy fluxes. *Sci. Data* **6**, 74 (2019).
72. Helbig, M. *Analysis of Boreal Peatland and Forest Evapotranspiration* (Zenodo, 2020); https://doi.org/10.5281/zenodo.3653056

Acknowledgements

The research published in this paper is part of the project titled Boreal Water Futures, which is funded by the Global Water Futures programme of the Canada First Research Excellence Fund; additional information is available at www.globalwaterfutures.ca. We thank all the eddy covariance flux tower teams for sharing their data and we are grateful to the ESM groups for providing their model output through CMIP5. We thank the World Climate Research Programme's Working Group on Coupled Modelling for leading the CMIP. We acknowledge the research group that made the peatland map freely available and we thank E. Chan (ECCC) for processing the shapefile PEATMAP to a raster map. We are grateful to E. Sahlée and A. Rutgersson for providing lake eddy covariance data to an earlier version of the manuscript, T. Zivkovic and S. Davidson for insightful feedback, and M. Khomik, A. Green, E. Kessel, G. Drewitt, P. Kolari and M. Provenzale for helping with data preparation. I.M. acknowledges funding from ICOS-FINLAND (grant no. 281255), the Finnish Center of Excellence (grant no. 307331) and the EU Horizon 2020 RINGO project (grant no. 730944). A.P. acknowledges funding through the research project no. 18–05–60203-Arktika (RFBR and Government of Krasnoyarsk Territory, Krasnoyarsk Regional Fund of Science) and support for flux tower sites RU-ZOP and RU-ZOB through the Max Planck Society. A.D. and J.T. acknowledge funding from US National Science foundation (grant no. DEB-1440297) and a DOE Ameriflux Network Management Project award to the ChEAS core site cluster. T.A.B., A.G.B. and R.J. acknowledge support received through grants from the Fluxnet Canada ResearchNetwork (2002–2007; NSERC, CFCAS and BIOCAP) and the Canadian Carbon Program (2008–2012; CFCAS) and by an NSERC (Climate Change and Atmospheric Research) grant to the Changing Cold Regions Network (CCRN; 2012–2016) and an NSERC Discovery Grant. H. I. and M. U. acknowledge support by the Arctic Challenge for Sustainability (ArCS) project. J.K. and A.V. acknowledge funding from RFBR project no. 19–04–01234-a. B.A. acknowledges funding through NASA, NSERC, BIOCAP Canada, the Canadian Foundation for Climate and Atmospheric Sciences and the Canadian Foundation for Innovation for flux measurements at CA-MAN and

through the Canadian Forest Service, the Natural Sciences and Engineering Research Council of Canada (NSERC), the FLUXNET-Canada Network (NSERC, the Canadian Foundation for Climate and Atmospheric Sciences (CFCAS) and BIOCAP Canada), the Canadian Carbon Program (CFCAS), Parks Canada, the Program of Energy Research and Development (PERD), and Action Plan 2000 for flux measurements at CA-SF1, CA-SF2 and CA-SF3. M.B.N, M.O.L, M.P. and J.C. gratefully acknowledge funding from the Swedish research infrastructures SITES and ICOS Sweden and research grants from Kempe Foundations, (grant no. SMK-1743); VR (grant no. 2018–03966) and Formas, (grant no. 2016–01289) and M.P. gratefully acknowledges funding from Knut and Alice Wallenberg Foundation (grant no. 2015.0047). M.W. and I.F. acknowledge funding by the German Research Foundation (grant no. Wi 2680/2–1) and the European Union (grant no. 36993). B.R. and L.K. acknowledge support by the Cluster of Excellence 'CliSAP' (EXC177) of the University of Hamburg, funded by the German Research Foundation. O.S. acknowledges funding by the Canada Research Chairs, Canada Foundation for Innovation Leaders Opportunity Fund, and Natural Sciences and Engineering Research Council Discovery Grant Programs. H.I. acknowledges JAMSTEC and IARC/UAF collaboration study (JICS) and Arctic Challenge for Sustainability Project (ArCS).

Author contributions

M.H. and J.M.W. designed the study. M.H., J.M.W. and J.R.M. developed the methodology. J.M.W., P.A., B.A., M.A., A.G.B., T.A.B., P.D.B., S.K.C, J.Chen, J.Chi, A.R.D., A.D., E.E., T.F., L.B.F., I.F., A.G., S.H., M.H., E.R.H., H.Ikawa, H.Iwata, P.-E.I., R.J., J.K., M.K., L.K., A.Lindroth, T.O., M.O.L., A.Lohila, T.M., I.M., P.M., P.A.M., D.F.N., E.M.N., M.B.N., M.P., R.M.P., R.P., A.P., W.L.Q., N.T.R., D.E.R., B.R.K.R., O.S., I.B.S., P.T., E.-S.T., J.-P.T., J.T., M.U., A.V., M.W., S.W. and V.Z. contributed eddy covariance flux data. M.H. analysed the data and wrote the first draft. All authors contributed to data interpretation and commented on the manuscript at all stages.

Competing interests

The authors declare no competing interests.

Additional information

Extended data is available for this paper at https://doi.org/10.1038/s41558-020-0763-7.

Supplementary information is available for this paper at https://doi.org/10.1038/s41558-020-0763-7.

Correspondence and requests for materials should be addressed to M.H.

Peer review information *Nature Climate Change* thanks Claire Treat and the other, anonymous, reviewer(s) for their contribution to the peer review of this work.

Reprints and permissions information is available at www.nature.com/reprints.

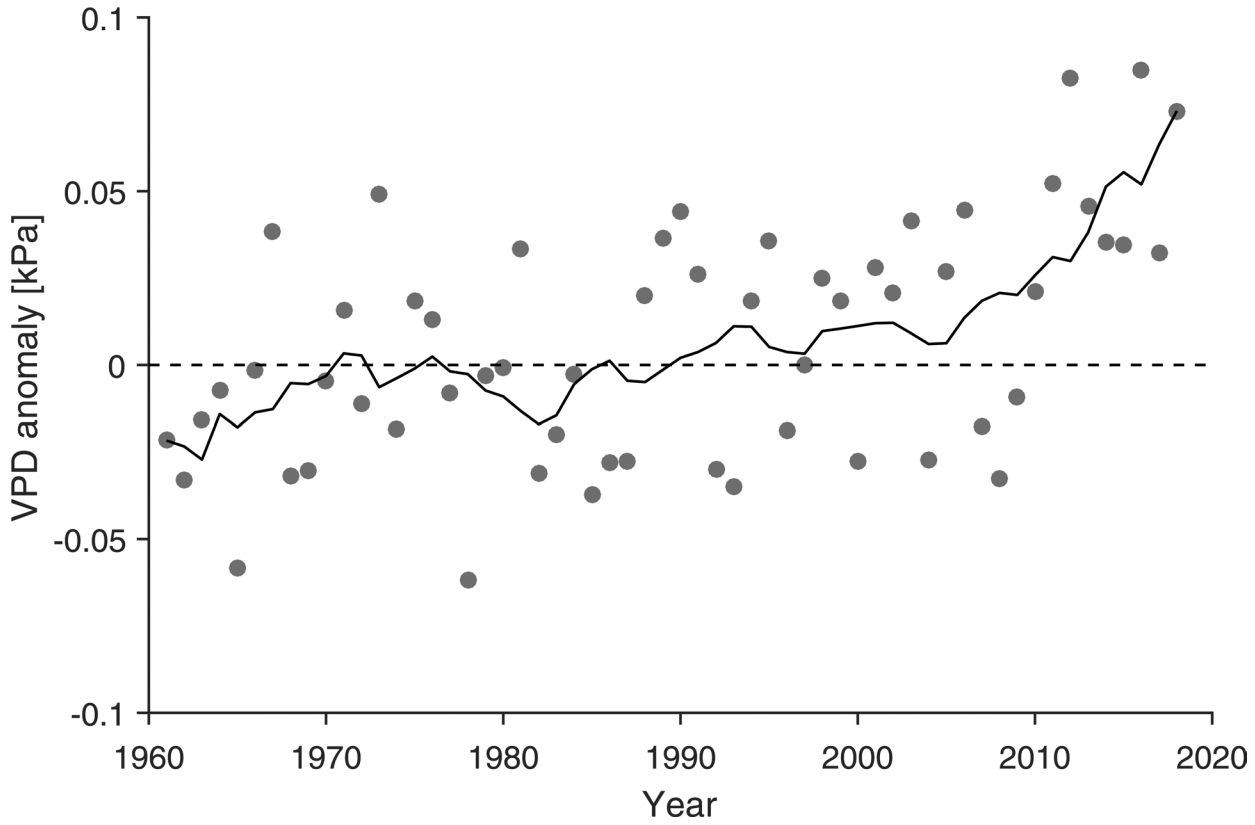

Extended Data Fig. 1 | Anomalies of growing season (May-September) mean daily maximum vapour pressure deficit (VPD_{GS}) for the boreal biome (circles, relative to the mean of 1981–2010). The solid line shows five-year running mean. VPD_{GS} is derived from the University of East Anglia Climate Research Unit [CRU] TS v4.03 dataset (Methods) and boreal biome grid cells are identified based on ref. [59].

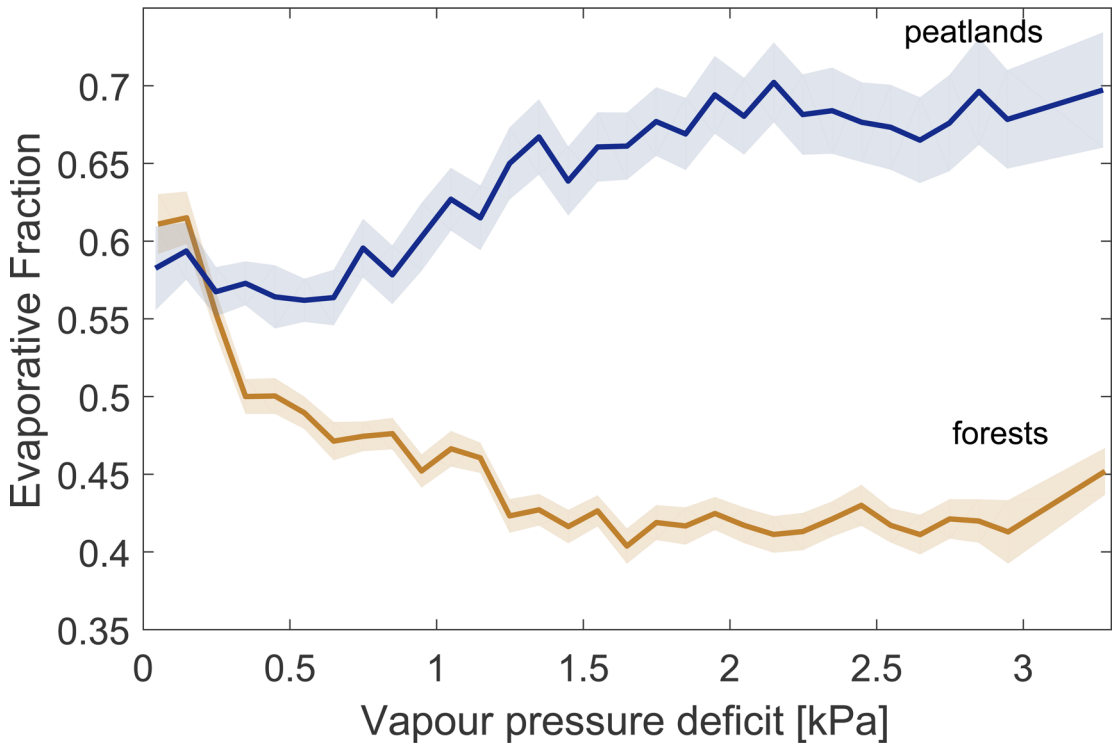

Extended Data Fig. 2 | Relationship between observed half-hourly afternoon (15h-18h) evaporative fraction and vapour pressure deficit for forest and peatland sites during the growing season. Shaded areas show standard errors.

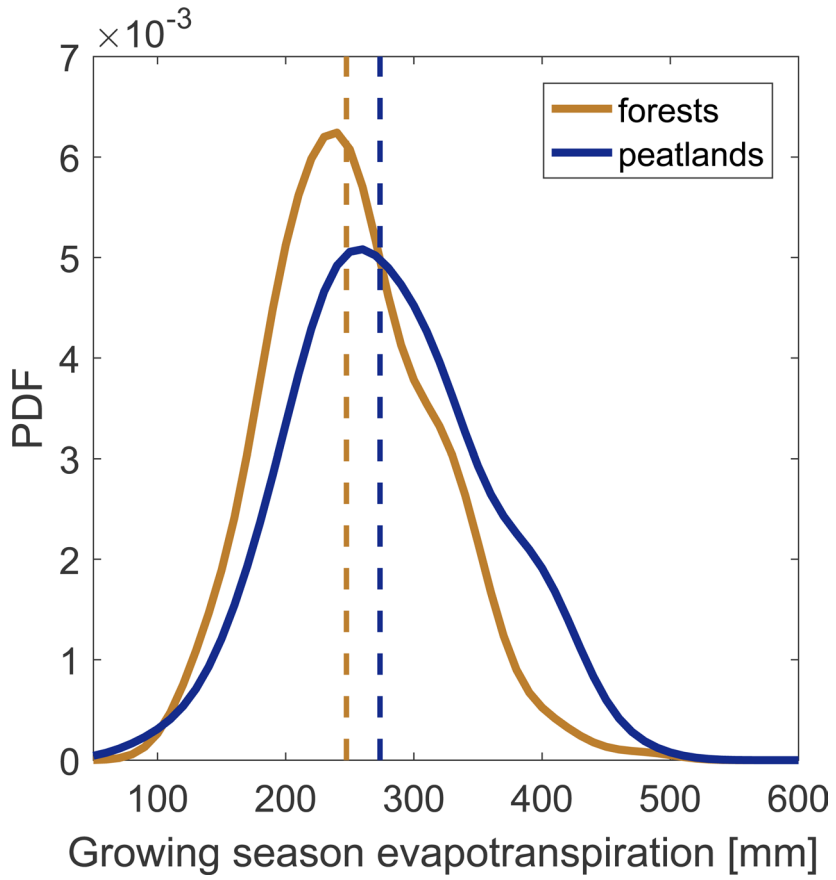

Extended Data Fig. 3 | Probability density function (PDF, solid lines) of observed growing season (May- September) forest ($n = 305$ growing seasons) and peatland ($n = 122$ growing seasons) evapotranspiration. Dashed lines show median growing season evapotranspiration.